Molecular Cancer Therapeutics

Characterization of the Selective Indoleamine 2,3-Dioxygenase-1 (IDO1) Catalytic Inhibitor EOS200271/PF-06840003 Supports IDO1 as a Critical Resistance Mechanism to PD-(L)1 Blockade Therapy

Bruno Gomes[1], Gregory Driessens[1], Derek Bartlett[2], Danying Cai[3], Sandra Cauwenberghs[1], Stefano Crosignani[1], Deepak Dalvie[2], Sofie Denies[1], Christopher P. Dillon[2], Valeria R. Fantin[2], Jie Guo[2], Marie-Claire Letellier[1], Wenlin Li[2], Karen Maegley[2], Reece Marillier[1], Nichol Miller[2], Romain Pirson[1], Virginie Rabolli[1], Chad Ray[2], Nicole Streiner[2], Vince R. Torti[2], Konstantinos Tsaparikos[2], Benoit J. Van den Eynde[1,4], Martin Wythes[2], Li-Chin Yao[3], Xianxian Zheng[2], Joseph Tumang[2], and Manfred Kraus[2]

Abstract

Tumors use indoleamine 2,3-dioxygenase-1 (IDO1) as a major mechanism to induce an immunosuppressive microenvironment. IDO1 expression is upregulated in many cancers and considered to be a resistance mechanism to immune checkpoint therapies. IDO1 is induced in response to inflammatory stimuli such as IFNγ and promotes immune tolerance by depleting tryptophan and producing tryptophan catabolites, including kynurenine, in the tumor microenvironment. This leads to effector T-cell anergy and enhanced T_{reg} function through upregulation of FoxP3. As a nexus for the induction of key immunosuppressive mechanisms, IDO1 represents an important immunotherapeutic target in oncology. Here, we report the identification and characterization of the novel selective, orally bioavailable IDO1 inhibitor EOS200271/PF-06840003. It reversed IDO1-induced T-cell anergy *in vitro*. In mice carrying syngeneic tumor grafts, PF-06840003 reduced intratumoral kynurenine levels by over 80% and inhibited tumor growth both in monotherapy and, with an increased efficacy, in combination with antibodies blocking the immune checkpoint ligand PD-L1. We demonstrate that anti–PD-L1 therapy results in increased IDO1 metabolic activity thereby providing additional mechanistic rationale for combining PD-(L)1 blockade with IDO1 inhibition in cancer immunotherapies. Supported by these preclinical data and favorable predicted human pharmacokinetic properties of PF-06840003, a phase I open-label, multicenter clinical study (NCT02764151) has been initiated. *Mol Cancer Ther; 17(12); 2530–42. ©2018 AACR.*

Introduction

Immunotherapy has now been clinically validated as an effective approach for cancer therapy. Clinical trials with antibodies blocking cytotoxic T lymphocyte-associated antigen 4 (CTLA-4) and programmed cell death protein 1 (PD-1) or programmed cell death ligand 1 (PD-L1) have led the way to a second generation of immune checkpoint inhibitors (1). Most targets in the immuno-oncology field are costimulatory or coinhibitory receptors modulated through monoclonal antibody agonism or blockade, respectively. In addition, small molecules targeting intracellular mediators of tumor immune escape are now also being developed as cancer immunotherapeutics. Examples supported by increasing data include indoleamine 2,3-dioxygenase-1 (IDO1), RORγt, or certain protein kinases (2).

IDO1 is a heme-containing dioxygenase that catalyzes the oxidation of L-tryptophan to N'-formyl kynurenine in the first and rate-limiting step of tryptophan catabolism. N'-formyl kynurenine is subsequently converted by formamidase to L-kynurenine and additional downstream immunologically-active metabolites via the kynurenine pathway. IDO1 promotes peripheral antitumor immune tolerance (3). Its expression and activity are often elevated in the tumor microenvironment, typically in response to inflammatory stimuli such as IFNγ (4). The exact mechanisms by which IDO1 activity downregulates antitumor immunity are still unclear. They may involve sensing of tryptophan depletion via GCN2 kinase–mediated phosphorylation of eIF2a and mTOR. This initiates a stress response resulting in cell-cycle arrest of T cells

[1]iTeos Therapeutics SA, Gosselies, Belgium. [2]Pfizer Inc., San Diego, California. [3]The Jackson Laboratory, Sacramento, California. [4]Ludwig Institute for Cancer Research, de Duve Institute, Université catholique de Louvain, Brussels, Belgium.

Note: Supplementary data for this article are available at Molecular Cancer Therapeutics Online (http://mct.aacrjournals.org/).

B. Gomes and G. Driessens contributed equally to this article.

Corresponding Authors: Manfred Kraus, Pfizer Inc., 10774 Science Center Drive, San Diego, CA 92121. Phone: 858-622-7313; E-mail: Manfred.Kraus@Pfizer.com; and Gregory Driessens, iTeos Therapeutics SA, Rue Auguste Piccard 48, 6041 Gosselies, Belgium. Phone: 32-71-960152; E-mail: gregory.driessens@iteostherapeutics.com

doi: 10.1158/1535-7163.MCT-17-1104

(5, 6). In addition or alternatively, binding of L-kynurenine or its metabolites to the aryl hydrocarbon receptor (AhR) causes effector T-cell apoptosis or differentiation into immunosuppressive regulatory T cells (7–10).

IDO1 expression is associated with a poor prognosis in several cancer indications (11–14). As such, IDO1 is a target of high interest for cancer immunotherapy, and IDO1-inhibiting drugs have become a focus of research and development efforts for tumor immune therapy (15). Clinical trials with IDO1 pathway inhibitors are underway, including indoximod (d-1-methyl-tryptophan) and epacadostat (INCB024360). Among these, INCB024360 inhibits the catalytic activity of IDO1 (16–18). Here, we described the initial characterization of EOS200271/PF-06840003, a novel and selective, orally bioavailable IDO1 catalytic inhibitor with promising *in vivo* efficacy, and predicted human pharmacokinetic properties. In addition, we show a mechanistic link between anti–PD-L1 treatment and IDO1 activity, thereby implicating IDO1 as a critical driver of adaptive resistance to therapies targeting the PD-1/PD-L1 axis. Based on our findings, PF-06840003 was selected for further clinical evaluation in a phase I study.

Materials and Methods

Expression, purification, and enzymatic activity

Full-length cDNAs for human IDO1, indoleamine 2,3-dioxygenase 2 (IDO2), and tryptophan 2,3-dioxygenase (TDO2) were cloned into pFastbac-1 and for mouse and dog IDO1 into pET24a vectors. The inhibition of IDO1, IDO2, and TDO2 was measured by quantitating tryptophan and kynurenine by MS (details in Supplementary Methods).

Protein binding

PF-06840003 (same as EOS200271), PF-06840002, and PF-06840001 were synthesized as described (19). The protein binding of PF-06840002 and PF-06840001 was determined by equilibrium dialysis in pooled male and female mouse plasma by incubating PF-06840003 at 2 μmol/L.

Cell lines and culture conditions

HeLa (CCL-2, 2014), THP-1 (TIB-202, 2013), A172 (CRL-1620, 2014), SKOV3 (HTB-77, 2015), and MDA-MB-231 (HTB-26, 2014) human cell lines and B16-F10 (CRL-6475, 2010), CT26 (CRL-2638, 2014), EMT6 (CRL-2755, 2016), Renca (CRL-2947, 2013), and 4T1 (CRL-2539, 2016) mouse cell lines were purchased from the ATCC (ATCC-No, year obtained) and cultured according to their recommended conditions. The MC38 cell line was provided by Dr. Antoni Ribas (UCLA) in 2011. The murine PanO2 cell line was obtained from the NCI (Bethesda, MD). MC38 and PanO2 cells were cultured in RPMI with 10% FBS. P815 mTDO2 cl12 cells were generated and cultured as described (20). Cell lines routinely tested negative for Mycoplasma spp. contamination (MycoAlert, Lonza). ATCC verifies cell line identity with short tandem repeat (STR) analysis. Pfizer authenticated cell lines in their central cell bank by STR and interspecies contamination analysis that was performed at IDEXX BioResearch with the CellCheck 16 Plus – human and CellCheck Plus – mouse assays.

IDO1 catalytic activity cellular assays

Twenty thousand HeLa cells were seeded per well in 200 μL growth media in a 96-well plate and allowed to adhere overnight. Then, growth media were replaced with 200 μL reduced (2%) serum media containing 100 ng/mL IFNγ (R&D, 285-IF-100) and incubated for 48 hours to induce IDO expression. THP-1 cells (100,000) were seeded in 100 μL IMDM with 4% FBS, 100 ng/mL LPS (Sigma, L-4391), and 50 ng/mL IFNγ to induce IDO expression. In both assays, eleven 3-fold dilutions of compounds PF-06840003, PF-06840002, or PF-06840001 beginning at 50 μmol/L were added for 24 hours. Supernatant (100 μL) was transferred to a v-bottom 96-well plate. Note that 30 μL 30% trichloroacetic acid was added and centrifuged at 3,000 RPM for 10 minutes. Hundred microliter was transferred to a flat-bottom 96-well plate and combined with 100 μL of 2% 4-(dimethylamino)benzaldehyde in acetic acid to derivatize N-formyl kynurenine to kynurenine for quantitative colorimetric readout. Assay plates were read at A_{492} on an Envision plate reader (Perkin Elmer). IC_{50} values were calculated using Activity Base software (Version 8.0.5.4) and nonlinear regression of percent inhibition versus Log_{10} concentration of IDO inhibitor compound.

TDO2 catalytic activity cellular assays

A172 cells were incubated at 12,500 cells/well with increasing concentrations of compounds for 16 to 18 hours. THP-1 cells (100,000 cells/well) were stimulated with 2 ng/mL phorbol-myristate acetate (PMA) for 24 hours and then incubated for 24 hours with compounds. P815 mTDO2 cl12 cells (50,000 cells/well) were incubated for 16 to 18 hours with compounds. Kynurenine concentrations were determined as described above.

Coculture assay

SKOV3 cells were seeded in IMDM with 10%, 25%, or 50% of human serum (Sigma) with increasing concentrations of PF-06840003 and then irradiated (10,000 rad). Human peripheral blood mononuclear cells were isolated from buffy coats, purified by density gradient centrifugation using Lymphoprep (StemCell), stimulated with CD3/CD28 beads (Invitrogen) and hIL2 (Sigma) in IMDM with 10%, 25%, or 50% of human serum, for 15 minutes, and then added to the SKOV3 cells. All samples were done in duplicate for T-cell proliferation measurement and as a single tryptophan and kynurenine measurement. After an incubation of 24 hours, the tryptophan and kynurenine concentrations in conditioned medium were assessed using LC-MS/MS. ^{3}H-thymidine was added to the cocultures for another 24-hour incubation period. Thymidine incorporation was measured using a TopCount counter (Perkin Elmer). Data were fitted and EC_{50} determined by using the Prism software (GraphPad software Inc.). EC_{50} was defined as the concentration at which PF-06840003 half-maximally rescued human T-cell proliferation.

Human whole blood assay

The assay was performed as previously described (21). Heparinized whole human blood was treated with LPS (25 μg/mL; Sigma, L-4391) and IFNγ (100 ng/mL; R&D, 285-IF-100). PF-06840003 was prepared in DMSO and added to individual 200 μL blood aliquots in concentrations ranging from 0.01 to 100 μmol/L. The total DMSO concentration was 0.5%. After incubation for 20 hours, the samples were extracted with organic solvent. A 30 μL aliquot was precipitated with 270 μL acetonitrile/HPLC water (70:30), vortexed, and centrifuged at

3,220 × *g* for 15 minutes at 10°C. An aliquot of the supernatant organic solution was diluted in 0.1% formic acid and spiked with stable labeled isotopes of kynurenine and tryptophan as internal standards prior to analysis. PF-06840002, PF-06840003, and kynurenine were measured using a triple quadrupole mass spectrometer. The IC_{50} and IC_{90} calculations were conducted in GraphPad Prism.

In vivo experiments

Female BALB/c and C57BL/6 mice (aged 6–8 weeks) were purchased from Charles River or The Jackson Laboratory. Tumor cells were implanted s.c. in PBS; B16-F10 (2×10^5), CT26 (2.5×10^5), EMT-6 (2×10^5), MC38 (2×10^5), PanO2 (2.5×10^6), Renca (10^6). 4T1 (10^5) cells were implanted in PBS, and MDA-MB-231 (5×10^6) cells suspended in serum-free media mixed with matrigel (Corning Life Sciences) were implanted into mammary fat pads. Mice were randomized into treatment groups based on tumor size. The experimenters were not blinded to the group assignment during the study and when assessing the outcome. Tumors were measured 3 times per week. Tumor volume was calculated based on two-dimensional caliper measurement as 0.5 × length × width^2. Tumor growth inhibition (TGI) was determined by the formula: $\%TGI = [1 - (Vt_x - Vt_0/Vc_x - Vc_0)] \times 100$, where *Vc* and *Vt* are the geometric means of control and treated groups, respectively, X is day X on study, and 0 is initial day of dosing. Isolated plasma or tumor tissue was assessed by the Pfizer Pharmacokinetics (PK), Dynamics and Metabolism Department for exposures. Anti–PD-L1 (clone 10F.9G2), anti–CTLA-4 (clone 9D9), and anti-CD8 (clone YTS 169.4) mAbs were purchased from BioXCell. Antibodies were dosed i.p. PF-06840003 was resuspended in 0.5% HPMC-E4M/0.25%Tween-20/H2O (Methocel, Colorcon), and mice were treated qd, b.i.d., or t.i.d. by oral gavage. All procedures performed on these animals were in accordance with regulations and established guidelines and were reviewed and approved by Pfizer's Institutional Animal Care and Use Committee. Animals were sacrificed when the tumor size reached >2,000 mm^3. The EMT6 model study was conducted at CrownBio-Taicang. Humanized NOD-scid IL2rγ^{null} (NSG) mice were generated as previously described (22). Engrafted Hu-NSG mice from different HSC donors were randomized independently and assigned into each treatment group. All animal procedures were carried out according to guidelines established by the Institutional Animal Care and Use Committee at Jackson Laboratories.

Analysis of tumor-infiltrating immune cells and splenocytes

Twenty-four hours after the third antibody treatment, tumor single cell suspensions were generated with the mouse tumor dissociation kit (Miltenyi) following the manufacturer's instructions. Tumor-infiltrating immune cells were enriched by gradient centrifugation on Lymphoprep and washed in PBS. Cells were treated 3 hours in the presence of PMA, Ionomycin, Brefeldin A, and Monensin according to the manufacturer's protocol (Cell Stimulation Cocktail, eBiosciences). Cells were placed overnight at 4°C and stained using Livid dye (Life Technologies). Fc receptors were blocked by incubation with Fc Block (eBiosciences). APCeFluor780-conjugated anti-mouse CD45 (30F11), FITC-conjugated anti-mouse CD4 (RM4-5), PECy7-conjugated anti-mouse CD8a (53-6.7), APC-conjugated anti-mouse IFN-gamma (XMG1.2), and Cell Stimulation Cocktail kit were obtained from eBiosciences. Flow cytometry was performed on a MACSQuant (Miltenyi), and data were analyzed with FlowJo (BD).

Results

Enzymatic activity and IDO1 specificity

PF-06840003 is a racemic mixture of active (PF-06840002) and inactive (PF-06840001) enantiomers, which spontaneously epimerize to each other in plasma (Fig. 1A and B). After incubation of pure PF-06840002 in plasma *in vitro*, a significant amount of PF-06840002 is converted to PF-06840001 in the first 6 hours in all of the three species tested (~65% in humans, 42% in dogs, and 34% in mice). Equilibration is achieved in 6 hours in humans, but delayed in dogs and mice (19). Based on this low interconversion barrier, the racemic mixture PF-06840003 rather than pure active enantiomer PF-06840002 was used in the *in vivo* experiments described below.

Using a mass spectrometry (MS)–based enzymatic assay, IC_{50} values for PF-06840003 were similar for dog (0.59 μmol/L) and human (0.41 μmol/L) IDO1 enzyme forms (Table 1). PF-06840003 was however 3.8 times more potent for the human enzyme compared with mouse IDO1 (IC_{50} values of 0.4 μmol/L vs. 1.5 μmol/L, respectively). For the active enantiomer PF-06840002, IC_{50} values were similar for dog and human (0.20 μmol/L vs. 0.20 μmol/L, respectively), whereas the inhibition of the human enzyme was 3.7 times more potent than mouse (0.20 vs. 0.73 μmol/L). Up to 10 μmol/L of PF-06840001, the inactive enantiomer, showed no IDO1 inhibition of the human enzyme. In the enzymatic MS assay, neither PF-06840003 nor PF-06840002 (active) were competitive with tryptophan for binding to either dog or human IDO1. We conclude that PF-06840002 is the enantiomer that actively inhibits IDO1 catalytic function in a noncompetitive manner with the substrate tryptophan, whereas PF-06840001 (inactive) is not a catalytic IDO1 inhibitor.

PF-06840003 activity in cellular assays

IDO1 is not constitutively expressed in many cell lines, but can be induced by treatment with proinflammatory cytokines, such as IFNγ (23). This is analogous to the induction of IDO1 by inflammatory cues in the tumor microenvironment (24). PF-06840003 inhibited IFNγ-induced IDO1 cellular activity, resulting in reduced kynurenine production in both HeLa cervical carcinoma and monocytic THP-1 cells (Table 1).

As expected, the PF-06840003 racemate (IC_{50} = 1.8 μmol/L in HeLa, 1.7 μmol/L in THP-1) was less potent than the active enantiomer PF-06840002 (IC_{50} = 1.0 μmol/L in HeLa, 1.1 μmol/L in THP-1) in both cellular models. The inactive enantiomer PF-06840001 was much less active in both cellular assays (IC_{50} = 12.8 μmol/L and 5.8 μmol/L, respectively). Its measured activity likely reflects racemization to the active enantiomer in culture over time. The inhibition of cellular IDO1 activity in these studies was not due to a reduction in cell viability (Supplementary Fig. S1).

To better determine the relative potencies of IDO1 inhibition in humans for racemic PF-06840003 versus active enantiomer PF-06840002, we set up a human whole blood *ex vivo* Pharmacodynamic (PD) stimulation assay. Whole blood samples were treated with LPS and IFNγ to induce IDO1. The IC_{50}s found were 4.7 ± 2.5 μmol/L for PF-06840003 and 2.5 ± 1.6 μmol/L for total PF-06840002 (Table 1). This corresponds to an adjusted unbound fraction IC_{50} of 1.1 ± 0.7 μmol/L, because PF-06840002

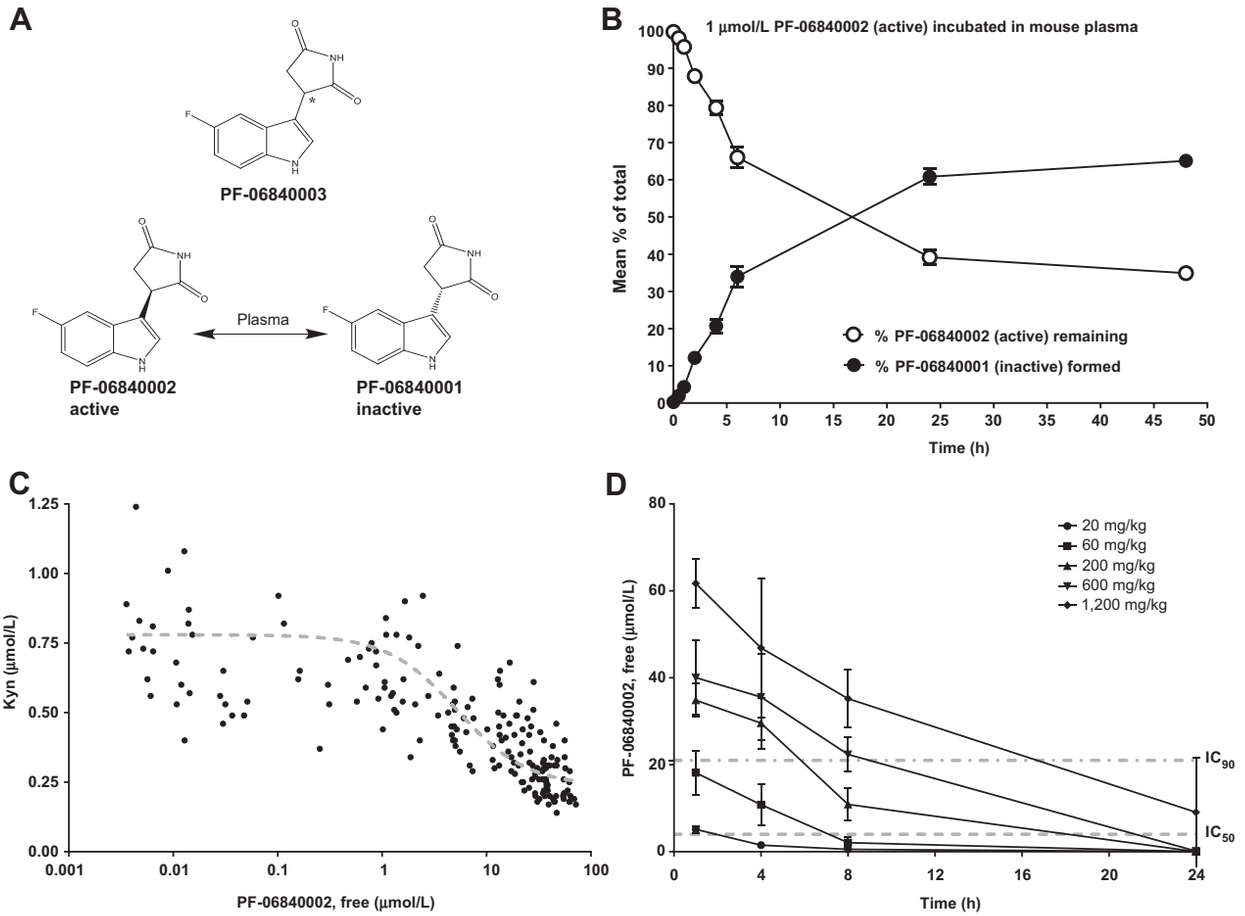

Figure 1.

PF-06840003: Structure + Racemate. **A,** Structure of PF-06840003 and its enantiomers PF-06840002 and PF-06840001. **B,** *In vitro* chiral interconversion. PF-06840003 is a racemate that equilibrates quickly in mouse plasma between PF-06840002, the active IDO1 inhibitor, and PF-06840001, which lacks the capacity to inhibit IDO1. Similar data were obtained in human and dog plasma (21). Data represent a triplicate analysis, mean ± SD shown. **C,** Correlation of plasma Kyn levels with PF-06840002 exposure in female BALB/c mice following a single oral dose of PF-06840003 as detailed in Supplementary Table S1. A four-parameter logistic equation with upper limit equal to 0.78 μmol/L (baseline Kyn in untreated mice), lower limit equal to 0.24 μmol/L (average Kyn level when free PF-06840002 > 50 μmol/L), and Hill coefficient equal to 1.3 (determined from the human whole blood assay) was used to estimate an *in vivo* IC_{50} of 5.2 μmol/L (dashed line). **D,** Mean plasma concentration vs. time of PF-06840002 following oral administration of PF-06840003 in female BALB/c mice. The mouse IDO1 IC_{50} and IC_{90} values extrapolated from the human whole blood assay (Table 1) are shown for reference. Error bars, SD.

has a high fraction unbound (fu) of 0.45. A summary of plasma protein binding and blood to plasma ratios is shown in Supplementary Table S1.

PF-06840003 is a selective IDO1 inhibitor

Next, we assessed whether PF-06840003 is selective for IDO1 over TDO2 and IDO2, the other two enzymes involved in tryptophan catabolism. PF-06840003, PF-06840002 (active), and PF-06840001 (inactive) were evaluated in recombinant TDO2 and IDO2 enzymatic assays and did not display any significant inhibitory activity toward mouse or human enzymes based on kynurenine production (Table 1).

In addition, we tested whether PF-06840003 inhibits TDO2 by assessing kynurenine production in three different TDO2-expressing cell lines. The human glioblastoma cell line A172 constitutively expresses TDO2, whereas in the human acute monocytic leukemia cell line THP1, TDO2 can be induced by treatment with PMA. The potential inhibition of murine TDO2 was evaluated in a P815 murine mastocytoma cell line transfected with a murine TDO2-expression plasmid. At concentrations up to 50 μmol/L, PF-06840003 did not display any significant inhibitory cellular activity toward human or mouse TDO2. Thus, PF-06840003 has strong selectivity for IDO1 among tryptophan-catabolizing enzymes.

PF-06840003 was further evaluated for off-target pharmacologic activity in a panel of 81 receptors, ion channels, transporters, and enzymes in a CEREP-wide ligand profile screen at a concentration of 200 μmol/L. Results indicated that PF-06840003 is highly selective. In the initial screen, significant interactions where PF-06840003 elicited >50% inhibition or agonism versus controls were limited to 3 targets (Supplementary Table S2). At 200 μmol/L melanocortin 2 receptor (functional antagonist; Kb = 170 μmol/L) showed 41% inhibition, the muscarinic M1 receptor (antagonist; Kb = 9.6 μmol/L) was 69% inhibited, and

Table 1. *In vitro* pharmacology of PF-06840003 and its enantiomers PF-06840002 and PF-06840001

Assay	PF-06840003	PF-06840002 (μmol/L)	PF-06840001
Enzyme activity[a]: IC_{50}			
Human IDO1	0.41 (0.30–0.54)	0.20 (0.16–0.26)	>10
Mouse IDO1	1.5 (1.3–1.7)	0.73 (0.70–0.76)	NT
Dog IDO1	0.59 (0.37–0.95)	0.20 (0.12–0.33)	NT
Human TDO2	>50	>50	>50
Mouse TDO2	>50	>50	>50
Human IDO2	>200		
Binding[a]			
Ferrous form			
Human IDO1; K_d^{app}	14 (12–16)	6 (3–12)	
Ferric form (-O_2)			
Human IDO1; K_d^{app}	0.32 (0.27–0.38)	0.16 (0.13–0.19)	
Cellular activity			
HeLa cells (+IFN**γ**)			
IDO1 IC_{50} ± SD (*n*)	1.8 ± 0.7 (13)	1.0 ± 0.4 (11)	12.8 ± 6.3 (5)
THP-1 cells (+IFNg/LPS)			
IDO1 IC_{50} ± SD (*n*)	1.7 ± 0.6 (9)	1.1 ± 0.4 (11)	5.8 ± 2.6 (5)
T-cell proliferation in SKOV3			
Coculture system (50% serum)		0.08 ± 0.05	
IDO1 EC_{50} ± SD ($n = 3$)			
A172, THP-1 and P815 mTDO2 cl12	No inhibition	No inhibition	No inhibition
TDO2	@50	@50	@50
Human whole blood assay			
IDO1 IC_{50} ± SD ($n = 10$); total	4.7 ± 2.5	2.5 ± 1.6	
Unbound		1.1 ± 0.7	
IDO1 IC_{90} unbound		5.7	

Abbreviations: Kd^{app} Ferrous, Kd^{app} when test article is titrated into the ferrous form of IDO1; Kd^{app} Ferric (+O_2), Kd^{app} when test article is titrated into the ferric form of IDO1 without measures to remove oxygen; Kd^{app} Ferric (- O_2), Kd^{app} when test article is titrated into the ferric form of IDO1 following oxygen depletion; Kd^{app} Ferric (-O_2, +Trp), Kd^{app} when test article is titrated into the ferric form of IDO1 following oxygen depletion in the presence of tryptophan; mIDO1, mouse IDO1 enzyme; NT, not tested; O_2, molecular oxygen; Trp, tryptophan.

[a]Data are represented as geometric mean in μmol/L, plus 95% confidence interval determined from 2 to 7 independent measurements.

monoamine oxidase A showed 51% inhibition (Supplementary Table S2). Follow-up titration curves determined an IC_{50} = 1.4 mmol/L for the melanocortin 2 receptor, an IC_{50} = 81 μmol/L for the muscarinic M1 receptor, and an IC_{50} = 190 μmol/L for monoamine oxidase A. Given the much lower IC_{50}s for IDO1 inhibition, these results suggest a low potential for secondary (off-target) pharmacology at clinically relevant exposures. Further supporting its exquisite selectivity, PF-06840003 did not show off-target activity against the EMD-Millipore KinaseProfiler panel of 270 kinases at 50 μmol/L.

The potential for cardiovascular impact, specifically QT prolongation, was tested using the hERG assay. This assay showed less than a 50% inhibition of the hERG channel up to 300 μmol/L, the highest concentration tested. Genotoxicity risk was assessed by a bacterial reverse mutation assay (Ames Test), and in an *in vitro* micronuclei test, the results of both tests were negative for genotoxicity (Supplementary Methods).

PF-06840003 rescues T-cell proliferation in coculture with immunosuppressive tumor cells

In vitro coculture of IDO1-expressing SKOV3 tumor cells and T lymphocytes was established to mimic the physiologic consequences of IDO1 expression in the tumor microenvironment on T-cell proliferation. Reduced T-cell proliferation in the presence of IDO1-positive tumor cells is used as a surrogate for the contribution of IDO1 to T-cell anergy in the tumor microenvironment. PF-06840003 effectively rescued IDO1-induced T-cell anergy in this assay with an EC_{50} of 80 nmol/L (Table 1; Supplementary Fig. S2A–S2C). IC_{50}s for inhibiting tryptophan to kynurenine conversion by SKOV3 cells in the same system were in the approximately 100 nmol/L range (Supplementary Fig. S2D–S2F), overall consistent with the values for overcoming T-cell inhibition. The ability of PF-06840003 to rescue T-cell proliferation appeared to be serum-independent with EC_{50} values from 60 to 74 nmol/L in serum concentrations ranging from 10% to 50%.

PF-06840003 inhibits IDO1 and blocks L-kynurenine formation *in vivo*

Modulation of IDO1 activity by PF-06840003 in nontumor-bearing BALB/c mice was determined by measurement of its effects on plasma L-kynurenine and tryptophan concentrations over time. Mice were orally administered a single dose of PF-06840003 ranging from 20 to 1200 mg/kg (Fig. 1D; Supplementary Table S3). L-kynurenine and tryptophan plasma concentrations in female BALB/c control mice were 0.78 ± 0.27 μmol/L and 90.7 ± 20.3 μmol/L, respectively (mean ± SD, $n = 65$). PF-06840003 administration caused a significant dose-dependent decrease of plasma L-kynurenine levels (Fig. 1C).

L-kynurenine reduction peaked at 1 hour post dose and correlated with concentrations of unbound active PF-06840002. A strong maximum reduction in plasma L-kynurenine (≥54 ± 6%) was observed at or above 200 mg/kg 1 hour after treatment. Based on the human whole blood assay and the 3.8-fold potency difference for inhibiting human versus mouse IDO1, the estimated *in vivo* IC_{50} and IC_{90} for free, unbound active PF-06840002 against mouse IDO1 are 4 μmol/L and 21 μmol/L, respectively.

Plasma L-kynurenine largely returned to or exceeded control levels by 24 hours after PF-06840003 administration. Interestingly, maximally reduced L-kynurenine levels are comparable with the observed lower plasma concentrations in IDO1

knock-out mice (25). We thus conclude that PF-06840003 can achieve transient complete inhibition of IDO1 catalytic activity in mice following oral administration.

Pharmacodynamics and antitumor activity of PF-06840003 in syngeneic mouse tumor models

A panel of syngeneic mouse tumor models was characterized for basal and posttreatment levels of the IDO1 substrate tryptophan and metabolite L-kynurenine in plasma and tumor (Table 2). Tumor presence caused normal or slightly elevated systemic plasma kynurenine levels compared with basal plasma levels of 0.78 ± 0.27 μmol/L kynurenine in BALB/c and 1.05 ± 0.28 μmol/L kynurenine in C57BL/6J nontumor-bearing control mice. Kynurenine concentrations varied widely across the tumor panel, with highest levels in MC38 and CT26 syngeneic tumor recipients. IDO1 inhibition with PF-06840003 treatment effectively lowered plasma kynurenine levels in tumor-bearing mice below basal levels. Similarly, a substantial reduction in kynurenine levels was achieved in tumor tissue across the panel (Table 2).

Next, we tested whether therapeutic IDO1 inhibition with PF-06840003 can suppress tumor growth across a panel of syngeneic models (PanO2, orthotopic 4T1, EMT6, Renca, B16-F10, CT26, MC38). We observed modest or transient TGI with PF-06840003 as a monotherapy (Fig. 2). No single-agent benefit was observed in the EMT6 breast cancer model.

In the CT26 colon carcinoma model with high IDO1 activity, a dose range and different dosing schedules were evaluated (Fig. 3A). Reductions in plasma L-kynurenine levels ($P < 0.0001$) were observed at all PF-06840003 treatment doses 3 hours after dosing and were sustained over 6 hours. A dose-dependent range of reduction occurred with a maximal reduction by 81 ± 14% at the highest dose (600 mg/kg b.i.d.). Tumor kynurenine levels were also significantly reduced ($P < 0.0001$) at 3 and 6 hours after dosing with PF-06840003. Maximal reduction of 93 ± 13% was achieved at the highest dose (600 mg/kg b.i.d.) and sustained 3 and 6 hours after treatment. We observed comparable TGI with PF-06840003 across the range of doses and dose schedules in the CT26 model (Supplementary Fig. S3).

Next, we tested whether the TGI with the IDO1 inhibitor PF-06840003 is immune-mediated. In the absence of $CD8^+$ T cells, IDO1 inhibition lost its impact on CT26 tumor growth (Supplementary Fig. S4).

Antitumor activity and pharmacodynamics of PF-06840003 in combination with immune checkpoint inhibition

Preclinical and clinical data both suggest that a greater antitumor benefit could be achieved when IDO1 inhibition is combined with immune checkpoint blockade (26, 27). Thus, much of the effort in the field has focused on identifying and validating various combination partners for IDO1 inhibition, such as antibodies that block PD-L1 (28). PD-L1 and related PD-L2 are ligands for PD-1, a member of the CD28 superfamily of costimulatory or -inhibitory T-cell receptors, that is mainly, but not exclusively, expressed on activated T cells. PD-1 ligand engagement limits T-cell proliferation and cytokine production. This is a key mechanism mediating T-cell peripheral tolerance. PD-1 engagement facilitates tumor progression, whereas inhibition of PD-1 signaling may enhance tumor immune surveillance and foster antitumor immune responses (29).

In order to test the effectiveness of combination therapy, PF-06840003 treatment was tested in combination with avelumab, a fully humanized PD-L1–blocking immunoglobulin G1 antibody, in the CT26 colorectal cancer syngeneic model. As described earlier for PF-06840003 monotherapy, a significant reduction of about 80% total tumor L-kynurenine content was observed in mice coadministered avelumab and PF-06840003 (Fig. 3A). As a single agent, L-kynurenine modulation by PF-06840003 resulted in a TGI of 41% (Fig. 3B and C). The combination of PF-06840003 with avelumab caused an improved TGI benefit of 74% (Fig. 3B and C).

Similar results were found for PF-06840003 combination with a rodent surrogate for the fully human avelumab, rat anti-mouse anti–PD-L1 mAb clone 10F.9G2 (Supplementary Fig. S5). When given as monotherapy, 10F.9G2 moderately delayed CT26 tumor growth. Combination of 10F.9G2 with PF-06840003 showed a significant benefit in inhibiting tumor growth versus anti–PD-L1 alone (Supplementary Fig. S5).

Immunodeficient mice engrafted with human $CD34^+$ hematopoietic stem cells develop partial human immune systems that are responsive to checkpoint inhibition therapy (22). We tested the effectiveness of PF-06840003 against human IDO1 in humanized NSG mice bearing MDA-MB-231 breast tumors in two experiments using different human donors, as engrafting with $hCD34^+$ cells from diverse donors recapitulates some of the heterogeneity in response of the patient population (Supplementary Figs. S6 and S7). In both cases, PF-06840003 and anti–PD-L1 monotherapies achieved significant TGI. Combination of avelumab with PF-006840003 caused a modest benefit in inhibiting tumor growth versus anti–PD-L1 alone (Supplementary Figs. S6 and S7).

IDO1 inhibitor PF-06840003 combination with PD-L1 blockade increases IFNγ-secreting tumor-infiltrating T cells

We next analyzed how PF-06840003 monotherapy or combination with anti–PD-L1 antibody (clone 10F.9G2) may affect systemic versus tumor-infiltrating immune cells. Proportions of granulocytic and monocytic MDSCs, $CD4^+$, $CD8^+$, and regulatory T cells were not significantly different between the treatment conditions in CT26 tumors (Supplementary Fig. S8). When T-cell activation was tested using an intracytoplasmic IFNγ readout, PF-06840003 monotherapy did not induce any change in the proportion of IFNγ-secreting T cells. In contrast, anti–PD-L1 monotherapy or combination with the IDO1 inhibitor was able to increase the proportion of splenic IFNγ-secreting $CD4^+$ and $CD8^+$ T cells (Fig. 3D). Interestingly, the effect of anti–PD-L1 disappeared when tested on T cells originating from the tumor microenvironment, suggesting the existence of a local immunosuppressive mechanism. In this situation, only the combination of PF-06840003 with anti–PD-L1 could induce a higher proportion of IFNγ-secreting T cells that correlated with improved treatment efficacy (Fig. 3D). We conclude that IDO1 activity in the tumor microenvironment suppresses the induction of T-cell antitumor activity following anti–PD-L1 treatment.

IDO1 and L-kynurenine levels are increased in T-cell immune checkpoint–treated tumors

To test the hypothesis whether IDO1 may function as a resistance mechanism at the tumor site following treatment with an immune checkpoint inhibitor, we studied whether IDO1 activity was directly altered in anti–PD-L1 or anti–CTLA-4-treated tumor-bearing mice. Interestingly, kynurenine levels were significantly

Table 2. Kynurenine levels in syngeneic mouse tumors and plasma following anti–PD-L1 administrations and at indicated times after PF-06840003 treatment

Tumor				Kynurenine (μmol/L)			
				IDO1i		PD-L1 + IDO1i	
Tumor model	Mouse strain	Control	PD-L1	2 or 3 hours	6 hours	2 or 3 hours	6 hours
				3 hours		3 hours	
CT26[a]	*BALB/c*	11.12 ± 6.21 ($n = 25$)	16.04 ± 5.35 ($n = 12$)*	1.69 ± 0.50 ($n = 11$)**	1.43 ± 0.56 ($n = 11$)**	2.52 ± 1.20 ($n = 4$)*	1.91 ± 0.84 ($n = 4$)**
				3 hours		3 hours	
MC38[a]	*C57BL/6*	3.23 ± 1.41 ($n = 18$)	11.10 ± 5.98 ($n = 17$)**	1.67 ± 1.48 ($n = 8$)*	2.27 ± 1.24 ($n = 8$)	2.63 ± 1.90 ($n = 4$)	2.34 ± 1.40 ($n = 4$)
				3 hours		3 hours	
Pan02[b]	*C57BL/6*	2.40 ± 1.11 ($n = 10$)	2.35 ± 1.07 ($n = 10$)	0.67 ± 0.49 ($n = 5$)**	2.23 ± 1.13 ($n = 5$)	1.60 ± 1.06 ($n = 5$)	0.92 ± 0.58 ($n = 5$)*
				3 hours	8 hours		
4T1[a]	*BALB/c*	1.82 ± 1.31 ($n = 40$)		0.82 ± 0.59 ($n = 13$)*	0.91± 0.66 ($n = 15$)*		
				2 hours		2 hours	
EMT6[a]	*BALB/c*	1.01 ± 0.42 ($n = 5$)	0.93 ± 0.29 ($n = 4$)	0.48 ± 0.17 ($n = 3$)*	0.55 ± 0.17 ($n = 4$)*	0.36 ± 0.03 ($n = 3$)*	0.44 ± 0.10 ($n = 3$)*
				2 hours			
B16-F10[b]	*C57BL/6*	0.92 ± 0.34 ($n = 15$)	0.76 ± 0.30 ($n = 15$)	0.49 ± 0.09 ($n = 4$)*	0.42 ± 0.15 ($n = 3$)*	0.58 ± 0.13 ($n = 4$)*	0.58 ± 0.16 ($n = 4$)*
				2 hours		2 hours	
Renca[b]	*BALB/c*	0.54 ± 0.58 ($n = 16$)	0.48 ± 0.30 ($n = 15$)	0.16 ± 0.06 ($n = 3$)		0.19 ± 0.05 ($n = 6$)	

Plasma				Kynurenine (μmol/L)			
				IDO1i		PD-L1 + IDO1i	
Tumor model	Mouse strain	Control	PD-L1	2 or 3 hours	6 hours	2 or 3 hours	6 hours
None	**BALB/c**	0.78 ± 0.27 ($n = 65$)					
None	**C57BL/6J**	1.05 ± 0.28 ($n = 30$)					
				3 hours		3 hours	
CT26[a]	*BALB/c*	1.12 ± 0.63 ($n = 25$)##	1.28 ± 0.42 ($n = 12$)	0.34 ± 0.09 ($n = 11$)**	0.35 ± 0.06 ($n = 11$)**	0.31 ± 0.08 ($n = 4$)*	0.40 ± 0.10 ($n = 4$)*
				3 hours		3 hours	
MC38[a]	*C57BL/6*	1.10 ± 0.36 ($n = 18$)ns	1.38 ± 0.61 ($n = 17$)*	0.48 ± 0.13 ($n = 8$)**	0.51 ± 0.18 ($n = 8$)**	0.61 ± 0.13 ($n = 4$)**	0.73 ± 0.29 ($n = 4$)*
				3 hours		3 hours	
Pan02[b]	*C57BL/6*	0.92 ± 0.15 ($n = 10$)ns	1.00 ± 0.19 ($n = 10$)	0.36 ± 0.13 ($n = 5$)**	0.48 ± 0.14 ($n = 5$)**	0.48 ± 0.25 ($n = 5$)**	0.48 ± 0.28 ($n = 5$)**
				3 hours	8 hours		
4T1[a]	*BALB/c*	0.85 ± 0.21 ($n = 25$)ns		0.44 ± 0.12 ($n = 10$)**	0.56 ± 0.10 ($n = 5$)**		
				2 hours		2 hours	
EMT6[a]	*BALB/c*	1.01 ± 0.29 ($n = 5$)#	1.01 ± 0.39 ($n = 4$)	0.57 ± 0.22 ($n = 3$)*	0.58 ± 0.23 ($n = 4$)*	0.33 ± 0.01 ($n = 3$)**	0.57 ± 0.11 ($n = 3$)*
				2 hours			
B16-F10[b]	*C57BL/6*	0.94 ± 0.32 ($n = 15$)ns	0.75 ± 0.21 ($n = 15$)	0.32 ± 0.04 ($n = 4$)**	0.39 ± 0.03 ($n = 3$)*	0.37 ± 0.10 ($n = 4$)**	0.56 ± 0.09 ($n = 4$)*
				2 hours		2 hours	
Renca[b]	*BALB/c*	0.92 ± 0.26 ($n = 16$)#	0.84 ± 0.27 ($n = 15$)	0.19 ± 0.03 ($n = 3$)**		0.29 ± 0.11 ($n = 6$)**	

NOTE: Mean ± SD is shown.

[a]Mice were treated with 200 mg/kg, b.i.d. of PF-06840003.

[b]Mice were treated with 600 mg/kg, b.i.d. of PF-06840003.

*, $P < 0.05$ and **, $P < 0.005$ by unpaired Student t test vs. control.

#, $P < 0.05$; ##, $P < 0.005$; and ns, not significant ($P > 0.05$) by unpaired Student t test vs. respective nontumor-bearing mouse strain control.

increased in MC38 and CT26 tumors after treatment with either anti–PD-L1 or anti–CTLA-4, respectively (Fig. 4A and B), implying a direct link with IDO1 enzymatic activity. Next, we performed a Nanostring mRNA expression profile analysis in the MC38 mouse syngeneic colon tumor model. In the nCounter mouse Pancancer immune profiling panel, Pdcd1 (PD-1) and IDO1 transcripts were strongly increased in the anti–PD-L1 treatment group, whereas IDO1 inhibition alone had no significant impact

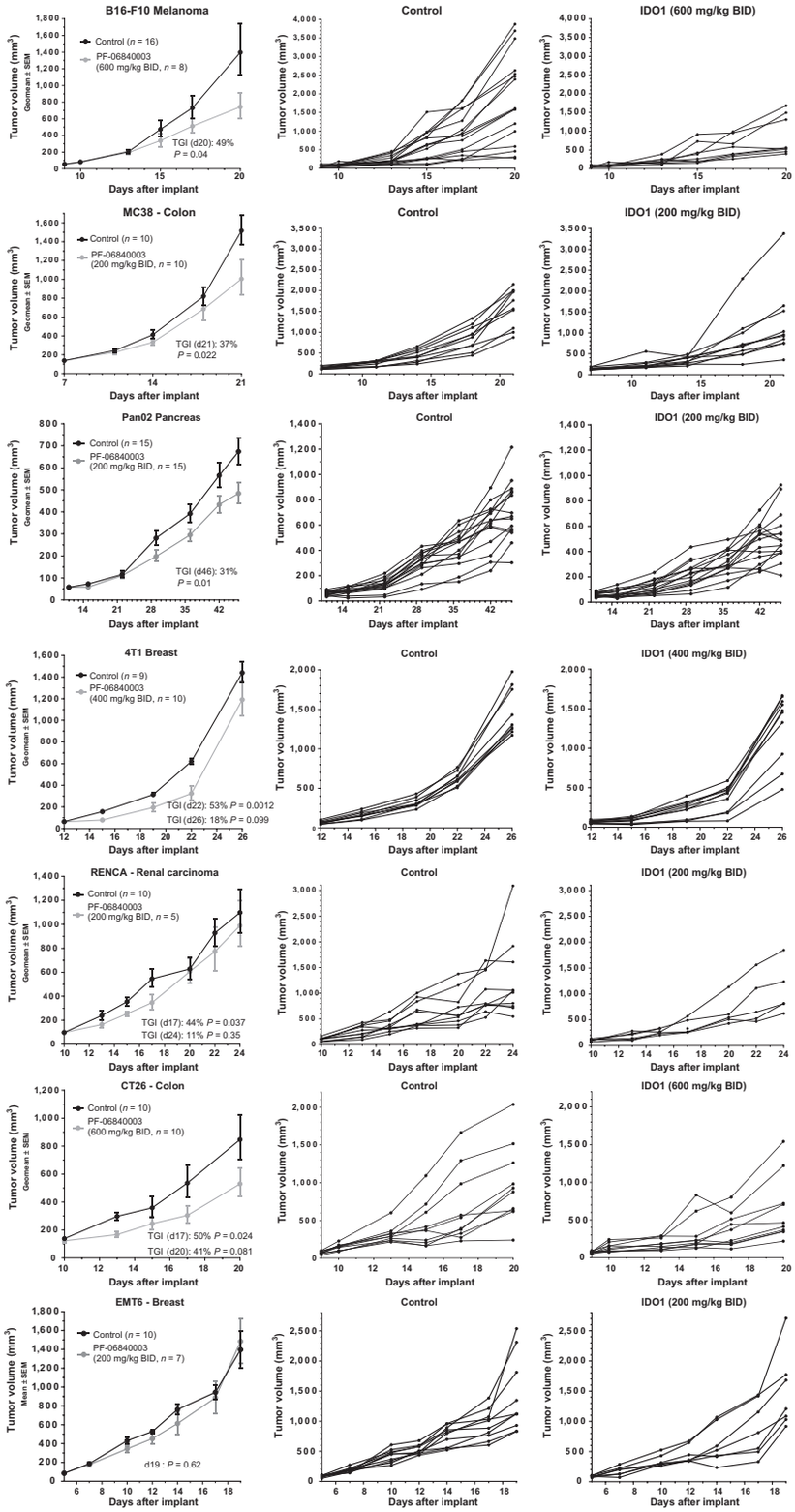

Figure 2.

IDO1 inhibition demonstrates significant antitumor growth benefit as monotherapy in syngeneic tumor models (ANCOVA). Mice were randomized into groups based on established tumor volume, and PF-06840003 treatment was initiated on the day after implantation as shown for each tumor model in the graphs. No single-agent IDO1 inhibitor antitumor efficacy was observed in the EMT6 breast model.

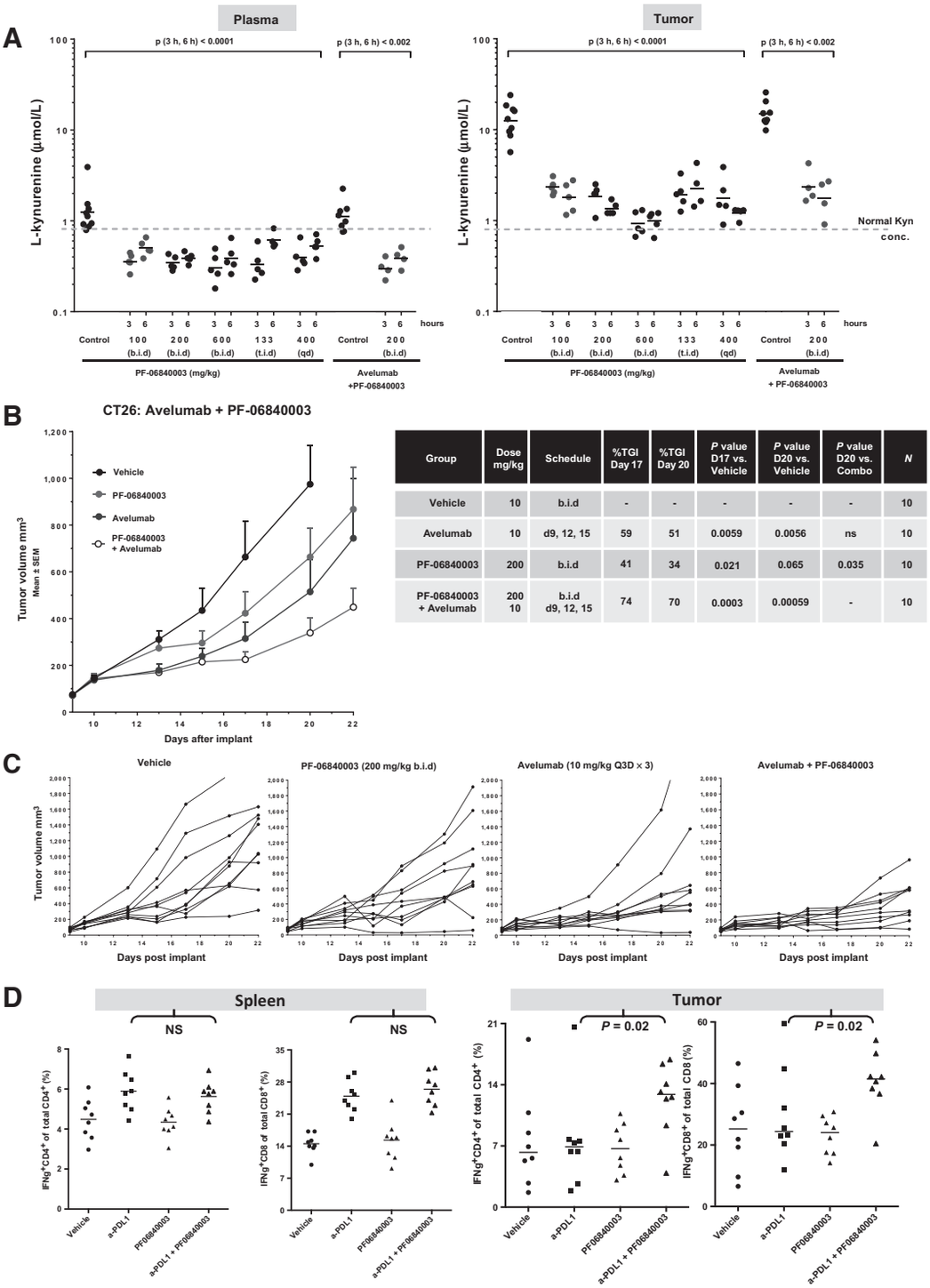

Group	Dose mg/kg	Schedule	%TGI Day 17	%TGI Day 20	*P* value D17 vs. Vehicle	*P* value D20 vs. Vehicle	*P* value D20 vs. Combo	*N*
Vehicle	10	b.i.d	-	-	-	-	-	10
Avelumab	10	d9, 12, 15	59	51	0.0059	0.0056	ns	10
PF-06840003	200	b.i.d	41	34	0.021	0.065	0.035	10
PF-06840003 + Avelumab	200 10	b.i.d d9, 12, 15	74	70	0.0003	0.00059	-	10

Figure 3.

Combinatorial IDO1i + avelumab (anti–PD-L1) treatment in the subcutaneous CT26 syngeneic mouse colon tumor model. **A,** PD modulation in CT26 tumors: Reduction of elevated Kyn levels in tumor tissue serves as a proximal PD biomarker for PF-06840003–mediated IDO1 inhibition. Plasma and tumor L-kynurenine and tryptophan concentrations were analyzed at 3 and 6 hours after the final dose. Plasma Kyn level in nontumor-bearing BALB/c mice is indicated by the gray dotted line. Statistical analysis: ANCOVA. **B,** TGI in mice. $n = 10$ per group; randomization and treatment start on day 9 after tumor implant. Statistical analysis: ANCOVA. **C,** Individual tumor growth curves. **D,** Increase of $CD4^+IFN\gamma^+$ and $CD8^+IFN\gamma^+$ T cells in CT26 tumors following combined anti–PD-L1 and PF-06840003 treatment. The proportion of splenic and intratumoral $CD4^+IFN\gamma^+$ and $CD8^+IFN\gamma^+$ T cells after 10 days of continuous PF-0684003 (200 mg/kg, b.i.d.) treatment and 3 doses of anti–PD-L1 (10 mg/kg; Q3D; clone 10F.9G2) is shown. Cells were stimulated for 3 hours in the presence of PMA/Iono/Brefeldin A. Line indicates the median. Statistical analysis is based on a two-way ANOVA test. $n = 8$ per group. Representative data of two independent experiments are shown.

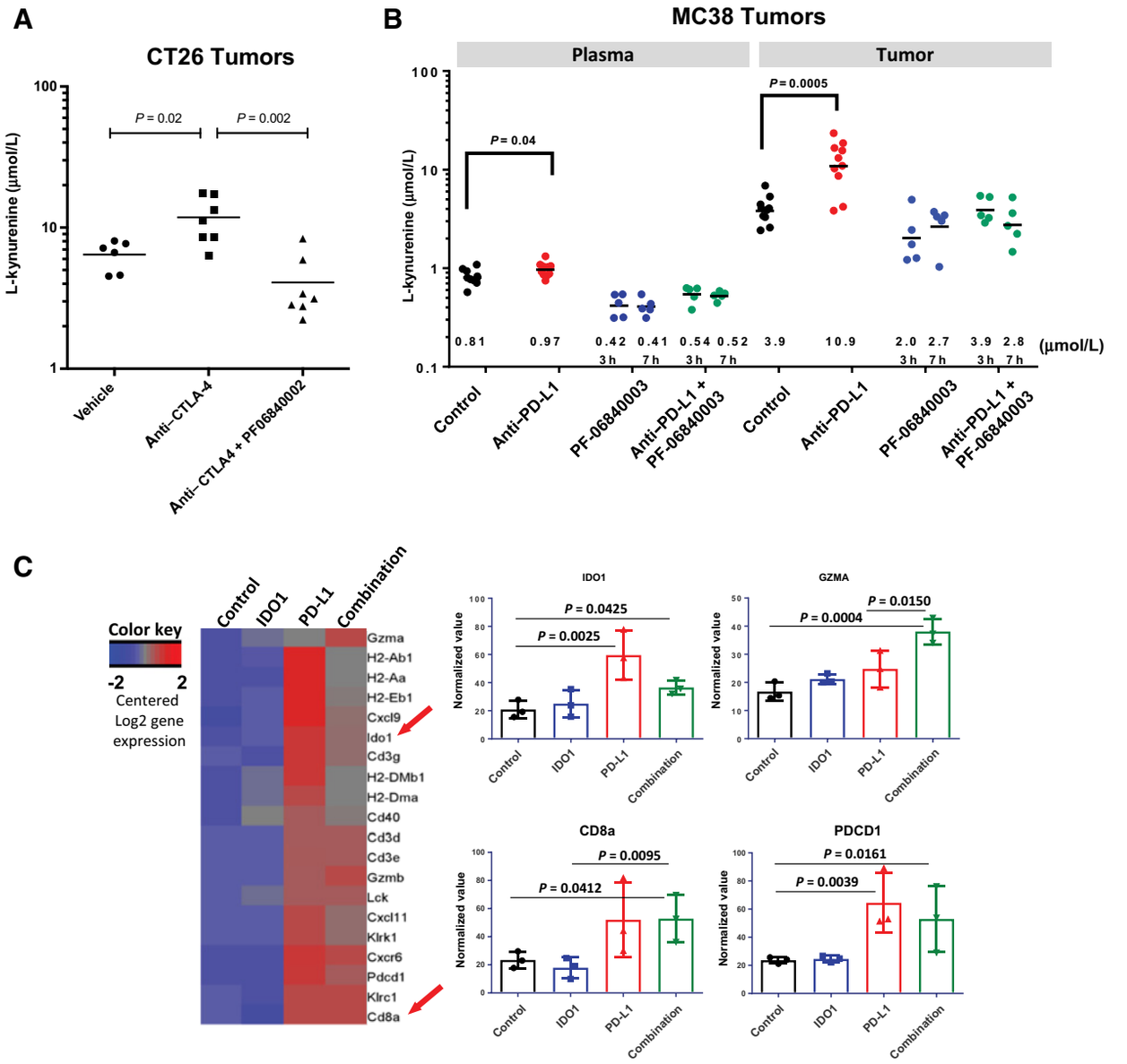

Figure 4.

Anti–PD-L1 and anti–CTLA-4 induce IDO1 activity as demonstrated in elevated Kyn levels in plasma and tumor tissue. **A,** PF-06840003 effectively suppresses anti–CTLA-4–induced elevated Kyn levels in CT26 tumors. Four hours past PF-06840002 dosage (100 mg/kg, b.i.d.). **B,** Elevated IDO1 activity/Kyn level in MC38 tumors following anti–PD-L1 (10F9G2) treatment. IDO1 inhibition counteracts the anti–PD-L1–driven upregulation of IDO1 activity demonstrated in lowered Kyn levels ($n = 10$ or 5; geomean shown; tumors were harvested on day 14 of treatment 3 or 7 hours after last IDO1i treatment). **C,** Increase of overall IDO1 expression in MC38 tumors after anti–PD-L1 treatment. Tumors ($n = 3$) were analyzed by nanostring technology on day 24 for quantification of gene expression transcript levels with the nCounter mouse Pancancer immune profiling panel. *P* values were calculated by one-way ANOVA analysis.

on its mRNA level (Fig. 4C). This establishes a direct mechanistic link between T-cell immune checkpoint inhibitor treatments in tumors with both the expression level and activity of IDO1 in the tumor microenvironment. Expression of the cytolytic enzyme granzyme A was increased after anti–PD-L1 + IDO1 inhibitor combination versus anti–PD-L1 monotherapy (Fig. 4C). This implies enhanced and/or extended antitumor activity in the presence of IDO1 inhibition. Taken together, these data support the hypothesis that IDO1 acts as an induced resistance mechanism to treatments targeting the PD-1/PD-L1 immune checkpoint node and provide additional mechanistic rationale to combine checkpoint-blocking therapeutics with an IDO1 inhibitor.

Discussion

PF-06840003 is a novel orally bioavailable IDO1 inhibitor. We have demonstrated selective PF-06840003 inhibitory activity on murine, dog, and human IDO1, whereas the other two

tryptophan-metabolizing enzymes TDO2 and IDO2 are not inhibited at physiologic concentrations of the drug. Inhibition of kynurenine production was also demonstrated in cervical carcinoma HeLa cells and in the THP-1 monocytic cell line. Exceptional selectivity for IDO1 and thus an overall low risk for off-target effects are further corroborated by CEREP-wide ligand profile and kinase panel screens.

Although the IC_{50} potency of the active enantiomer PF-06840002 in the enzymatic IDO1 assay does not reach the double-digit nanomolar range of the first described catalytic IDO1 inhibitor INCB024360 (17, 30), low plasma protein binding (Supplementary Table S1) coupled with favorable clearance and distribution characteristics provide a favorable human PK prediction for PF-06840002 (19).

We demonstrate that PF-06840003 is effective in modulating the Trp/Kyn balance *in vitro* and *in vivo* and able to rescue T-cell functions. Both tryptophan depletion and kynurenine metabolites have been described as important suppressors of T-cell function. T lymphocytes are sensitive to tryptophan shortage, which causes their arrest in the G_1 phase of the cell cycle (5). This cell-cycle arrest was proposed to depend on the induction of an integrated stress response triggered by the stress response kinase GCN2. GCN2 is activated by elevations in uncharged tRNAs and phosphorylates eIF2a leading to inhibition of protein translation (6). Recent data however did not confirm the role of GCN2 (31). Tryptophan depletion may also inactivate the mTOR pathway, although this was not demonstrated in lymphocytes so far (8). Another proposed mechanism of IDO1-mediated immune suppression involves the accumulation of tryptophan metabolites. 3-hydroxyanthranilic and quinolinic acids can induce T-cell apoptosis (10, 32), whereas other kynurenine derivatives can induce the differentiation of regulatory T cells (33). The AhR may mediate these inhibitory properties of kynurenine derivatives (9). We have used systemic and intratumor L-kynurenine concentrations as the most proximal pharmacodynamic biomarker of IDO1 activity and inhibition by PF-06840003, both *in vitro* and *in vivo*, and established a PK/PD relationship in mouse plasma.

The characterization of a panel of commonly used syngeneic mouse tumors revealed a wide spread for basal L-kynurenine levels in tumors of untreated mice, with MC38 and CT26 having the highest basal L-kynurenine levels. Because the syngeneic tumors do not express TDO2 (34) and PF-06840003 treatment effectively lowered L-kynurenine levels, IDO1 activity appears responsible for immunosuppressive tryptophan depletion and L-kynurenine generation in the murine tumor microenvironment.

Interestingly, the presence of mouse tumors did not result in a major significant systemic increase of L-kynurenine plasma concentrations across the syngeneic tumor panel versus nontumor-bearing controls. In human patients with advanced cancer however, serum levels of L-kynurenine were found to be increased (17). This could be due to relatively higher IDO1 activity in human versus mouse tumors and thus a more important role for IDO1 in suppressing the immune response against human tumors. PF-06840003 demonstrated an antitumor monotherapy benefit against established, randomized tumors in syngeneic tumor models, as well as in humanized mice bearing a human breast tumor. TGI was modest in some syngeneic models with variable or transient individual tumor growth delay benefits across the treatment groups. We thus tested PF-06840003 in a combination treatment setting, which holds higher promise for providing long-lasting antitumor efficacy.

We show that following treatment with immune checkpoint modulators, anti–CTLA-4 and anti–PD-L1 tumor IDO1 activity was significantly increased. This provides additional mechanistic rationale for combining these therapeutics with an IDO1 inhibitor.

IDO1's inherent main biological function is to prevent or terminate excessive immune activation. IDO1 expression is upregulated by type 1 and type 2 IFNs, which are frequently found at sites of inflammation (4). We show here that anti–CTLA-4 therapy increased kynurenine production in CT26 tumors. Efficacy of anti–CTLA-4 therapy was previously shown to be significantly increased in IDO1 knock-out mice (28). Although IDO1 was proposed to be a resistance mechanism to anti–CTLA-4 therapy with modulation of immune cell infiltrates (28), it had not been shown that anti–CTLA-4 could directly increase IDO1-dependent kynurenine production in tumors. We also found that anti–PD-L1 therapy induced both IDO1 expression and function in MC38 tumors. This further supports the mechanistic rationale for the clinical combination of anti–PD-(L)1 treatments with IDO1 inhibitors. The induction of IDO1 expression by anti–CTLA-4 and anti–PD-L1 is most likely indirect, resulting from T-cell activation which in turn induces secretion of IFNγ, a strong IDO1 inducer.

The therapeutic benefit of combining anti–PD-(L)1 therapy with IDO1 inhibition was already shown in previous publications (26, 28). Holmgaard and colleagues used 1-MT, a noncatalytic activity targeting IDO1 pathway inhibitor, in their *in vivo* studies. Spranger and colleagues performed pharmacologic studies with a potent IDO1 inhibitor derived from the clinical-stage compound INCB024360. Expanding beyond this work, our results help to understand the mechanism of action of the combination benefit of PF-06840003 and anti–PD-L1 antibody in two tumor models. The *in vivo* antitumor efficacy of PD-L1 blockade was associated with an increase in IFNγ-positive tumor-infiltrating lymphocytes. Interestingly, although anti–PD-L1 monotherapy induced a systemic increase in IFNγ-positive T cells as observed in the spleen, this anti–PD-L1 effect was lost at the tumor site and could only be rescued by combining anti–PD-L1 with PF-06840003. PF-06840003 efficiently decreased the anti–PD-L1-induced kynurenine production. These data indicate that although anti–PD-L1 induces a systemic T-cell activation, immunosuppressive mechanisms present within the tumor microenvironment prevent the efficacy of immune checkpoint inhibitors at the tumor site. The observation that IFNγ and IDO1 as well as kynurenine are induced within the tumor after treatment with anti–PD-L1 further confirms the activation of the IDO1 expression as a negative-feedback loop of anti–PD-L1 immunotherapy. For these reasons, our data support that PF-06840003 can promote and maintain a tumor-specific immune response by preventing IDO1-induced immunosuppressive mechanisms. Beyond our findings with anti–PD-L1, Monjazeb and colleagues have shown that several other immunotherapies such as IL2, anti-CD40, or CpG are promoting IDO1 expression in tumors (35).

Our phenotyping of the tumor immune infiltrate has not revealed any modification of regulatory T cells and myeloid-derived suppressor cells in PF-06840003–treated tumors (either in monotherapy or in combination with anti–PD-L1). The IDO1 inhibitor 1-MT was shown to modulate both effector and regulatory T cells in various syngeneic tumor models (28, 36).

Collective results obtained with potent and selective IDO1 inhibitors (PF-06840003 in this study, and the IDO1 inhibitor used by Spranger and colleagues) rather show and support a mechanism of action based on a marked increase of tumor-infiltrating effector T cells. Given the relatively low potency of 1-MT to directly inhibit IDO1's catalytic activity (17), other mechanisms have been proposed such as mTOR pathway inactivation (8). The difference in the potency and selectivity profiles of the IDO1 inhibitors used might explain the above-described differences in mechanism of action between the three different studies.

Beyond the preclinical data described here, PF-06840003 has a favorable predicted human PK profile. After oral administration of PF-06840003 to humans, the active enantiomer PF-06840002 has a predicted CLp of 0.64 mL/min/kg, Vss of 1.03 L/kg, and bioavailability of 64%. Central nervous system (CNS) distribution was investigated in male rats. Unbound AUC ratios of brain to plasma and cerebrospinal fluid (CSF) to plasma of PF-06840002 (active) were 0.20 and 0.49, and for PF-06840001 (inactive) were 0.21 and 0.56, respectively (19). These results indicate that CNS compartments are accessible to provide a promising treatment approach for brain metastases and glioblastoma with PF-06840003.

Disclosure of Potential Conflicts of Interest

S. Crosignani has ownership interest (including stock, patents, etc.) in iTeos Therapeutics SA. B. van den Eynde has ownership interest (including stock, patents, etc.) in, and is a consultant and advisory board member for, iTeos Therapeutics. M. Wythes and M. Kraus have ownership interest (including stock, patents, etc.) in Pfizer. No potential conflicts of interest were disclosed by the other authors.

Authors' Contributions

Conception and design: B. Gomes, G. Driessens, S. Cauwenberghs, S. Crosignani, V.R. Fantin, K. Maegley, R. Marillier, M. Wythes, M. Kraus

Development of methodology: D. Cai, S. Cauwenberghs, J. Guo, W. Li, K. Maegley, N. Miller, C. Ray, B. van den Eynde, X. Zheng

Acquisition of data (provided animals, acquired and managed patients, provided facilities, etc.): G. Driessens, D. Cai, S. Cauwenberghs, S. Denies, M.-C. Letellier, R. Marillier, N. Miller, R. Pirson, V. Rabolli, N. Streiner, V.R. Torti, K. Tsaparikos, L.-C. Yao

Analysis and interpretation of data (e.g., statistical analysis, biostatistics, computational analysis): B. Gomes, G. Driessens, D. Bartlett, D. Cai, S. Cauwenberghs, S. Denies, C.P. Dillon, V.R. Fantin, J. Guo, W. Li, K. Maegley, R. Marillier, N. Miller, R. Pirson, C. Ray, N. Streiner, V.R. Torti, B. van den Eynde, X. Zheng, M. Kraus

Writing, review, and/or revision of the manuscript: B. Gomes, G. Driessens, D. Bartlett, S. Crosignani, C.P. Dillon, J. Guo, W. Li, N. Miller, V.R. Torti, J. Tumang, M. Kraus

Administrative, technical, or material support (i.e., reporting or organizing data, constructing databases): D. Cai, D. Dalvie, M.-C. Letellier, N. Miller

Study supervision: B. Gomes, D. Cai, S. Cauwenberghs, N. Streiner, M. Wythes, M. Kraus

Acknowledgments

We are grateful to Paul Rejto, Bob Abraham, Martin Edwards, Katti Jessen, James Hardwick, Kenneth Hook, James G. Keck, Jenny Chaplin, Jay Srirangam, Shibing Deng, Conglin Fan, Hui Wang, Karsten Sauer, Erick Kindt, Stephanie Shi, Tao Zhang, Michel Detheux, Coraline De Maeseneire, Kim Frederix, Julie Preillon, and Pauline Bottemane for their generous support and helpful scientific discussions.

iTeos is supported by the Walloon region of Belgium and the FEDER (European Fund for Economic and Regional Development).

The costs of publication of this article were defrayed in part by the payment of page charges. This article must therefore be hereby marked *advertisement* in accordance with 18 U.S.C. Section 1734 solely to indicate this fact.

Received November 8, 2017; revised March 21, 2018; accepted September 12, 2018; published first September 19, 2018.

References

1. Mahoney KM, Rennert PD, Freeman GJ. Combination cancer immunotherapy and new immunomodulatory targets. Nat Rev Drug Discov 2015;14:561–84.
2. Iyer VV. Small molecules for immunomodulation in cancer: a review. Anticancer Agents Med Chem 2015;15:433–52.
3. Uyttenhove C, Pilotte L, Theate I, Stroobant V, Colau D, Parmentier N, et al. Evidence for a tumoral immune resistance mechanism based on tryptophan degradation by indoleamine 2,3-dioxygenase. Nat Med 2003;9:1269–74.
4. Mellor AL, Munn DH. IDO expression by dendritic cells: tolerance and tryptophan catabolism. Nat Rev Immunol 2004;4:762–74.
5. Munn DH, Shafizadeh E, Attwood JT, Bondarev I, Pashine A, Mellor AL. Inhibition of T cell proliferation by macrophage tryptophan catabolism. J Exp Med 1999;189:1363–72.
6. Munn DH, Sharma MD, Baban B, Harding HP, Zhang Y, Ron D, et al. GCN2 kinase in T cells mediates proliferative arrest and anergy induction in response to indoleamine 2,3-dioxygenase. Immunity 2005;22:633–42.
7. Bessede A, Gargaro M, Pallotta MT, Matino D, Servillo G, Brunacci C, et al. Aryl hydrocarbon receptor control of a disease tolerance defence pathway. Nature 2014;511:184–90.
8. Metz R, Rust S, Duhadaway JB, Mautino MR, Munn DH, Vahanian NN, et al. IDO inhibits a tryptophan sufficiency signal that stimulates mTOR: a novel IDO effector pathway targeted by D-1-methyl-tryptophan. Oncoimmunology 2012;1:1460–8.
9. Mezrich JD, Fechner JH, Zhang X, Johnson BP, Burlingham WJ, Bradfield CA. An interaction between kynurenine and the aryl hydrocarbon receptor can generate regulatory T cells. J Immunol 2010;185:3190–8.
10. Terness P, Bauer TM, Rose L, Dufter C, Watzlik A, Simon H, et al. Inhibition of allogeneic T cell proliferation by indoleamine 2,3-dioxygenase-expressing dendritic cells: mediation of suppression by tryptophan metabolites. J Exp Med 2002;196:447–57.
11. Okamoto A, Nikaido T, Ochiai K, Takakura S, Saito M, Aoki Y, et al. Indoleamine 2,3-dioxygenase serves as a marker of poor prognosis in gene expression profiles of serous ovarian cancer cells. Clin Cancer Res 2005;11:6030–9.
12. Brandacher G, Perathoner A, Ladurner R, Schneeberger S, Obrist P, Winkler C, et al. Prognostic value of indoleamine 2,3-dioxygenase expression in colorectal cancer: effect on tumor-infiltrating T cells. Clin Cancer Res 2006;12:1144–51.
13. Godin-Ethier J, Hanafi LA, Piccirillo CA, Lapointe R. Indoleamine 2,3-dioxygenase expression in human cancers: clinical and immunologic perspectives. Clin Cancer Res 2011;17:6985–91.
14. van Baren N, Van den Eynde BJ. Tumoral immune resistance mediated by enzymes that degrade tryptophan. Cancer Immunol Res 2015;3:978–85.
15. Platten M, von Knebel Doeberitz N, Oezen I, Wick W, Ochs K. Cancer immunotherapy by targeting IDO1/TDO and their downstream effectors. Front Immunol 2014;5:673.
16. Beatty GL, O'Dwyer PJ, Clark J, Shi JG, Bowman KJ, Scherle PA, et al. First-in-human phase I study of the oral inhibitor of indoleamine 2,3-dioxygenase-1 epacadostat (INCB024360) in patients with advanced solid malignancies. Clin Cancer Res 2017;23:3269–76.
17. Liu X, Shin N, Koblish HK, Yang G, Wang Q, Wang K, et al. Selective inhibition of IDO1 effectively regulates mediators of antitumor immunity. Blood 2010;115:3520–30.
18. Lob S, Konigsrainer A, Zieker D, Brucher BL, Rammensee HG, Opelz G, et al. IDO1 and IDO2 are expressed in human tumors: levo- but not dextro-1-methyl tryptophan inhibits tryptophan catabolism. Cancer Immunol Immunother 2009;58:153–7.

19. Crosignani S, Bingham P, Bottemanne P, Cannelle H, Cauwenberghs S, Cordonnier M, et al. Discovery of a novel and selective indoleamine 2,3-dioxygenase (IDO-1) inhibitor 3-(5-Fluoro-1H-indol-3-yl)pyrrolidine-2,5-dione (EOS200271/PF-06840003) and its characterization as a potential clinical candidate. J Med Chem 2017;60:9617–29.
20. Pilotte L, Larrieu P, Stroobant V, Colau D, Dolusic E, Frederick R, et al. Reversal of tumoral immune resistance by inhibition of tryptophan 2,3-dioxygenase. Proc Natl Acad Sci U S A 2012;109:2497–502.
21. Newton RC, Scherle PA, Bowman K, Liu X, Beatty GL, O'Dwyer PJ, et al. Pharmacodynamic assessment of INCB024360, an inhibitor of indoleamine 2,3-dioxygenase 1 (IDO1), in advanced cancer patients. J Clin Oncol 2012;30(15 suppl):2500.
22. Wang M, Yao LC, Cheng M, Cai D, Martinek J, Pan CX, et al. Humanized mice in studying efficacy and mechanisms of PD-1-targeted cancer immunotherapy. FASEB J 2018;32:1537–49.
23. Takikawa O, Kuroiwa T, Yamazaki F, Kido R. Mechanism of interferon-gamma action. Characterization of indoleamine 2,3-dioxygenase in cultured human cells induced by interferon-gamma and evaluation of the enzyme-mediated tryptophan degradation in its anticellular activity. J Biol Chem 1988;263:2041–8.
24. Muller AJ, Sharma MD, Chandler PR, Duhadaway JB, Everhart ME, Johnson BA 3rd, et al. Chronic inflammation that facilitates tumor progression creates local immune suppression by inducing indoleamine 2,3 dioxygenase. Proc Natl Acad Sci U S A 2008;105:17073–8.
25. Koblish HK, Hansbury MJ, Bowman KJ, Yang G, Neilan CL, Haley PJ, et al. Hydroxyamidine inhibitors of indoleamine-2,3-dioxygenase potently suppress systemic tryptophan catabolism and the growth of IDO-expressing tumors. Mol Cancer Ther 2010;9:489–98.
26. Spranger S, Koblish HK, Horton B, Scherle PA, Newton R, Gajewski TF. Mechanism of tumor rejection with doublets of CTLA-4, PD-1/PD-L1, or IDO blockade involves restored IL-2 production and proliferation of CD8 (+) T cells directly within the tumor microenvironment. J Immunother Cancer 2014;2:3.
27. Gangadhar TC, Hamid O, Smith DC, Bauer TM, Wasser JS, Olszanski AJ, et al. Epacadostat plus pembrolizumab in patients with advanced melanoma and select solid tumors: updated phase I results from ECHO-202/KEYNOTE-037. Ann Oncol 2016;27(suppl 6):1110PD–PD.
28. Holmgaard RB, Zamarin D, Munn DH, Wolchok JD, Allison JP. Indoleamine 2,3-dioxygenase is a critical resistance mechanism in antitumor T cell immunotherapy targeting CTLA-4. J Exp Med 2013;210:1389–402.
29. Chen L, Han X. Anti-PD-1/PD-L1 therapy of human cancer: past, present, and future. J Clin Invest 2015;125:3384–91.
30. Yue EW, Douty B, Wayland B, Bower M, Liu X, Leffet L, et al. Discovery of potent competitive inhibitors of indoleamine 2,3-dioxygenase with in vivo pharmacodynamic activity and efficacy in a mouse melanoma model. J Med Chem 2009;52:7364–7.
31. Sonner JK, Deumelandt K, Ott M, Thome CM, Rauschenbach KJ, Schulz S, et al. The stress kinase GCN2 does not mediate suppression of antitumor T cell responses by tryptophan catabolism in experimental melanomas. Oncoimmunology 2016;5:e1240858.
32. Fallarino F, Grohmann U, Vacca C, Bianchi R, Orabona C, Spreca A, et al. T cell apoptosis by tryptophan catabolism. Cell Death Differ 2002;9:1069–77.
33. Fallarino F, Grohmann U, You S, McGrath BC, Cavener DR, Vacca C, et al. The combined effects of tryptophan starvation and tryptophan catabolites down-regulate T cell receptor zeta-chain and induce a regulatory phenotype in naive T cells. J Immunol 2006;176:6752–61.
34. Xing F, Qian W, Dong C, Xu X, Guo S, Shi Q. Abstract 5597: Genomic profiling of syngeneic mouse cell lines and *in vitro* screen of the models against checkpoint inhibitors and target agents for preclinical application. Cancer Res 2017;77(13 suppl):5597.
35. Monjazeb AM, Kent MS, Grossenbacher SK, Mall C, Zamora AE, Mirsoian A, et al. Blocking indolamine-2,3-dioxygenase rebound immune suppression boosts antitumor effects of radio-immunotherapy in murine models and spontaneous canine malignancies. Clin Cancer Res 2016;22:4328–40.
36. Holmgaard RB, Zamarin D, Li Y, Gasmi B, Munn DH, Allison JP, et al. Tumor-expressed IDO recruits and activates MDSCs in a Treg-dependent manner. Cell Rep 2015;13:412–24.